Experimental and Theoretical Studies of the Phenyl Radical Reaction with Propene

J. Park, G. J. Nam,† I. V. Tokmakov,‡ and M. C. Lin*

Department of Chemistry, Emory University, Atlanta, Georgia 30322

Received: April 19, 2006; In Final Form: May 22, 2006

The kinetics for the reaction of C_6H_5 with propene has been measured by cavity ring-down spectrometry (CRDS) at temperatures 296−496 K under an Ar pressure of 40 Torr. The total rate constant can be given by the following Arrhenius expression (in units of $cm^3\ mol^{-1}\ s^{-1}$): $k(C_6H_5 + C_3H_6) = 10^{11.93\pm0.06}\ \exp[-(1512 \pm 51)/T]$. Density functional and higher level of theory calculations (up to the G2M level) have been carried out to provide additional insights about the mechanism of this reaction, and we also performed transition state theory (TST) calculation for the rate constant prediction. Our theoretical kinetic calculations predict that the C_6H_5 addition to the terminal $=CH_2$ site in propene is dominant at the temperature range of our CRDS measurements. However, the H-abstraction channel forming benzene and the allyl radical becomes increasingly important at higher temperatures. The total high-pressure limiting rate constant calculated on the basis of the G2M reaction barriers is in reasonable agreement with the experimental values.

Introduction

Reactions of aryl radicals with unsaturated hydrocarbons are of interest to the formation and molecular growth pathways for the polycyclic aromatic hydrocarbons (PAH) in various environments ranging from hydrocarbon flames[1−4] to the photospheres of carbon-rich stars.[5,6] Detailed kinetic modeling of the PAH formation requires thermodynamic and kinetic parameters for the reactions of aryl radicals with various unsaturated hydrocarbons. Instead of obtaining all this information from direct experiments, it is desirable to estimate the necessary parameters by simple and effective computational tools benchmarked against the accurate experimental and theoretical results for the prototypical reactions, for example, the phenyl radical reactions with small (C_2 and C_3) unsaturated hydrocarbons.

In our earlier studies, we used experimental[7] and computational[8,9] tools to elucidate the mechanism and provide accurate thermodynamic and kinetic data for the gas-phase reactions of C_6H_5 with C_2H_2 and C_2H_4. Recently, our group[10] and others[11−13] have also studied the mechanism and kinetics for the reactions of C_6H_5 with C_3H_4 isomers (propyne and allene). In this study, we will apply both experimental and theoretical methodologies to investigate the reaction of C_6H_5 with propene. Hefter et al.[14] studied this reaction back in 1972 by electron spin resonance (ESR). The experiments were carried out at 183 K in liquid propene. The predominant reaction mode was shown to be the C_6H_5 addition to the terminal carbon atom; the second possible addition product ($C_6H_5(CH_3)CHCH_2$) and the H-atom abstraction product (allyl radical) were also observed in the ESR spectrum. However, no kinetic data is available for the reaction of C_6H_5 with propene.

In the following section, we report the first direct measurement of the total rate constant for the title reaction by the cavity ring-down spectrometry (CRDS). The interpretation of the experimental results will be given on the basis of density functional and higher-level electronic structure computations, which provide molecular and energetic parameters for the reactants, products, transition states, and reactive intermediates. The latter theoretical parameters are used to calculate product distribution and the total rate constant that can be correlated with experimental data.

Results and Discussion

A. Kinetic Measurements by CRDS. The experimental apparatus and kinetic data acquisition by CRDS have been discussed in our previous publications,[7] only a brief description will be given here. Two pulsed lasers were employed for the photolysis and probe processes. A Lambda Physik LPX 105E excimer laser was used to photodissociate C_6H_5NO (nitrosobenzene) at 248 nm. A tunable pulsed dye laser pumped by a XeCl excimer laser (Lambda Physik FL 3002) was employed for probing C_6H_5 at 504.8 nm, where a distinct absorption peak was known to exist.[15,16] C_6H_5NO (Aldrich, 97%) was recrystallized from ethanol and vacuum-dried. Then it was placed on a sintered glass fritted disk inside a sealed mixing tube and carried into the reactor by a through flow of Ar gas (Matheson, 99.995% UHP grade). The C_6H_5 decay signals with and without added C_3H_6 reactant (Matheson, 99.5% CP grade, purified by trap-to-trap distillation) were measured with a Hammamatsu photomultiplier and acquired and averaged with a multichannel digital oscilloscope (LeCroy 9310M). The averaged signals were transferred to a microcomputer for storage and further analysis. A pulse delay generator (SR DG535), interfaced with computer, was used to control the delay time between the two laser firings as well as the triggering of the oscilloscope. The lasers were typically operated at 4 Hz. The temperature of the reactor was controlled by resistive heating and measured using a K-type thermocouple placed a few millimeters below the central axis of the reactor. The amount of C_3H_6 and the carrier gas were precisely measured with calibrated MKS mass flowmeters.

The kinetics for the reaction of C_6H_5 with propylene has been measured by CRDS at temperatures 296−496 K under an Ar pressure of 40 Torr. The pseudo-first-order rate constants of

* To whom correspondence should be addressed. E-mail: chemmcl@emory.edu.

† Also at Institute for Advanced Engineering, Yongin P.O. Box 25, Kyonggi-do, 449-863, South Korea.

‡ Present Address: Department of Chemistry, University of Missouri-Columbia, Columbia, MO 65211.

10.1021/jp062413d CCC: $33.50
Published on Web 06/23/2006

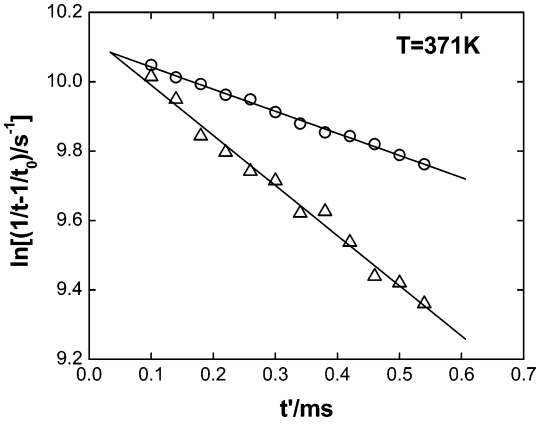

Figure 1. Typical pseudo-first-order decay plots for the $C_6H_5 + C_3H_6$ reaction in the presence of different excess amounts of C_3H_6: (○) $[C_3H_6] = 0$; (△) $[C_3H_6] = 5.41 \times 10^{-8}$ mol cm^{-3}. The slopes of these plots give the first-order decay constants k'.

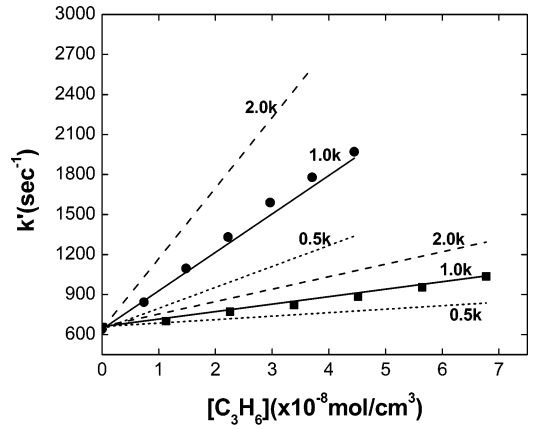

Figure 2. k' vs $[C_3H_6]$ at 296 K (■) and 451 K (●). Linear least-squares fit yields the second-order rate constants (k) for the $C_6H_5 + C_3H_6$ reaction. Lines are kinetically modeled results.

the C_6H_5 decay (k') were determined from the decay times of the probing photons in the absence (t^0) and presence (t) of the C_6H_5 radicals (the only species with strong absorption at 504.8 nm), using the following kinetic relationship[7]

$$\ln(1/t - 1/t^0) = A - k't'$$

which defines the functional dependence of t from the time delay t' between the photolysis and probe laser firings. Figure 1 presents typical plots of $\ln(1/t - 1/t^0)$ vs t' at 340 K in the presence of different amounts of C_3H_6. For a given concentration of C_3H_6, A and k' were obtained by a linear weighted least-squares analysis of the corresponding $\ln(1/t - 1/t^0)$ vs t' plot. Parameter A is an experimental constant, which contains geometric and optic characteristics of the reactor.

The second-order plots of k' vs $[C_3H_6]$ are presented in Figure 2. The slopes of these plots give the bimolecular rate constants for the $C_6H_5 + C_3H_6$ reaction. The experimental values obtained for the temperature range 296−451 K at 40 Torr Ar pressure are summarized in Table 1. They can be accurately represented by the following Arrhenius expression (in units of cm^3 mol^{-1} s^{-1})

$$k(C_6H_5 + C_3H_6) = 10^{11.93\pm0.06} \exp[-(1512 \pm 51)/T]$$

We have also examined the effect of pressure on the reaction at 383 K by varying the total pressure from 40 to 120 Torr. As shown in Figure 3, the effect is negligible under the conditions studied.

TABLE 1: Measured Bimolecular Rate Constants[a] for the $C_6H_5 + C_3H_6$ Reaction

T (K)	P (Torr)	[RH][b]	k
296	40	0−6.78	0.56 ± 0.02
340	40	0−5.90	0.92 ± 0.03
371	40	0−5.41	1.47 ± 0.05
383	40	0−5.16	1.80 ± 0.06
383	120	0−5.16	1.68 ± 0.07
400	40	0−5.01	2.03 ± 0.07
422	40	0−4.75	2.29 ± 0.08
451	40	0−4.45	3.05 ± 0.10
496	40	0−4.04	3.99 ± 0.31

[a] Rate constants are given in units of 10^{10} cm^3 mol^{-1} s^{-1}, and their associated errors represent one standard deviation. [b] Given in units of 10^{-8} mol cm^{-3}.

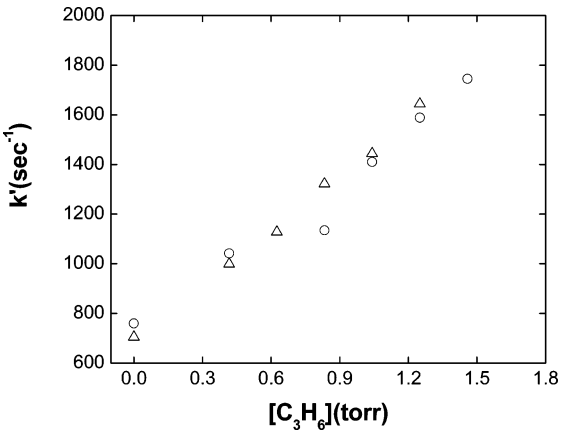

Figure 3. Pressure dependence of k' at 383 K: $P = 40$ Torr (△); $P = 120$ Torr (○).

The kinetics for the decay of C_6H_5 radicals whose concentrations are typically in the range of 5−15% of the initial C_6H_5-NO concentration ($1-8 \times 10^{-11}$ mol cm^{-3}) within the CRDS cavity has been simulated recently using the reaction mechanism in Table 2 with a set of C_6H_5 reactions including the molecular reaction of interest and radical processes (e.g., C_6H_5 + NO, $C_6H_5 + C_6H_5$, and $C_6H_5 + C_6H_5NO$) whose kinetics are well-established.[17,18] As shown in Figure 2, the second-order kinetics could be quantitatively modeled using the SENKIN program,[19] and Figure 2 also illustrates the sensitivity of the k value to the slope in the second-order plot. Our sensitivity analysis illustrated in Figure 4 clearly indicates that the C_6H_5 radical is predominantly affected by the $C_6H_5 + C_3H_6$ reaction. The key function of the SENKIN program is to compute the value of a sensitivity coefficient (S_{ij}) which reflects the degree of influence by a particular reaction j on any species (i) of interest—reactants, products, or reactive intermediates—as a function of reaction time. The sensitivity coefficient is defined by $S_{ij} = (\partial C_i/\partial k_j)(k_j/C_i)$, where C_i is the concentration of the ith species and k_j is the rate constant of the jth reaction included in the mechanism.

B. Reaction Mechanism and Product Branching. Additional density functional and higher level of theory calculations have been carried out with the Gaussian 03[20] and Molpro 2002[21] suites of programs for those regions of the $[C_9H_{11}]$ potential energy surface (PES) that are relevant to the $C_6H_5 + C_3H_6$ reaction. Molecular structures of the reactants, products, transition states, and intermediates were optimized using the B3LYP hybrid gradient-corrected density functional of Becke[22] with the 6-311++G(d,p) basis set. No geometric constraints were applied during the optimization calculations, which were done using

TABLE 2: Reactions and Rate Constants Used in the Modeling of the $C_6H_5 + C_3H_6$ Reaction in the CRD Experiment

reactions	A	n	E_a	reference[b]
1a. $C_6H_5+C_3H_6 \rightarrow CH_3CHCH_2C_6H_5$	1.7×10^{04}	2.47	735	this work
1b. $C_6H_5+C_3H_6 \rightarrow CH_2CH(C_6H_5)CH_3$	1.6×10^{03}	2.64	1680	this work
1c. $C_6H_5+C_3H_6 \rightarrow C_6H_6+C_3H_5$	1.4×10^{00}	3.82	1440	this work
2. $C_3H_5+C_3H_5 \rightarrow C_3H_5C_3H_5$	1.0×10^{13}	0	−260	*c*
3. $C_6H_5+C_3H_5 \rightarrow C_9H_{10}$	1.0×10^{13}	0	0	*d*
4. $C_6H_5NO \rightarrow C_6H_5+NO$	1.4×10^{17}	0	55100	
5. $C_6H_5+NO \rightarrow C_6H_5NO$	3.0×10^{12}	0	−860	
6. $C_6H_5+C_6H_5NO \rightarrow C_{12}H_{10}+NO$	5.0×10^{12}	0	4500	
7. $C_6H_5+C_6H_5 = C_{12}H_{10}$	2.4×10^{13}	0	111	
8. $C_6H_5+C_6H_5O \rightarrow C_{12}H_{10}O$	1.0×10^{13}	0	0	
9. $C_6H_5+C_{12}H_{10}N \rightarrow C_{18}H_{15}N$	1.0×10^{13}	0	0	
10. $C_6H_5+C_6H_5NO \rightarrow C_{12}H_{10}NO$	4.9×10^{12}	0	−68	
11. $C_{12}H_{10}NO+C_6H_5 \rightarrow C_{12}H_{10}N+C_6H_5O$	1.0×10^{13}	0	0	
12. $C_{12}H_{10}N+NO \rightarrow C_{12}H_{10}NNO$	1.0×10^{13}	0	0	
13. $C_{12}H_{10}NO \rightarrow C_6H_5NO+C_6H_5$	5.0×10^{14}	0	45000	

[a] Rate constants are defined by $k = AT^n \exp(-E_a/RT)$ and in units cm^3, mol, and s; E_a is in units of cal mol^{-1}. [b] Reference 17 unless otherwise noted. [c] Reference 18. [d] Estimated from reactions 2 and 7.

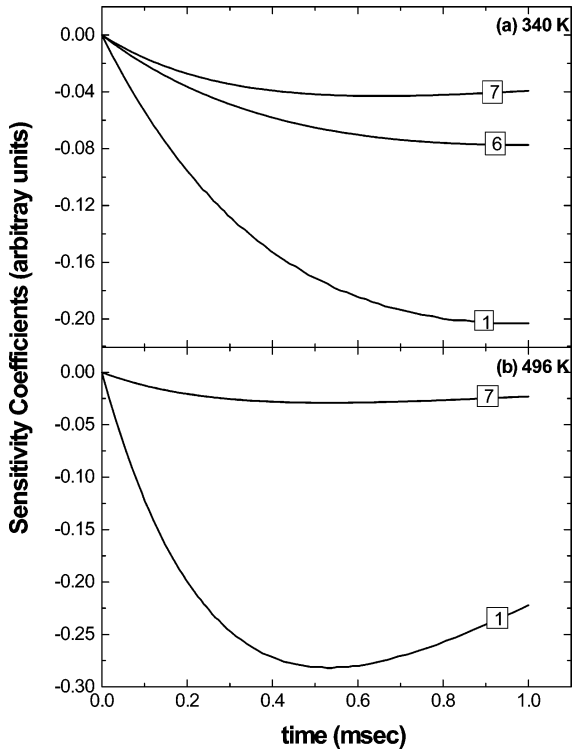

Figure 4. Sensitivity analysis for the $C_6H_5 + C_3H_6$ reaction at $P = 40$ Torr. The conditions are $[C_6H_5]_0 = 4.5 \times 10^{-12}$ mol/cm^3, $[C_6H_5NO] = 4.1 \times 10^{-11}$ mol/cm^3, and $[C_3H_6] = 5.9 \times 10^{-7}$ mol/cm^3 at 301 K and $[C_6H_5]_0 = 3.2 \times 10^{-12}$ mol/cm^3, $[C_6H_5NO] = 1.3 \times 10^{-11}$ mol/cm^3, and $[C_3H_4] = 4.0 \times 10^{-8}$ mol/cm^3 at 496 K. The reaction numbers are given in Table 2 (see the text for the definition of sensitivity coefficient).

the analytical gradient-based Berny[23] and modified GDIIS[24] algorithms. Harmonic vibrational frequencies calculated at the same level of theory were used without any adjustments for zero-point energy (ZPE) corrections, characterization of the stationary points as minima or saddle points, and rate constant calculations. The assignment of the transition states to the elementary reactions was routinely done by a visual inspection of atomic movements in the vibrational modes associated with imaginary frequencies. For the key channels, we have also optimized the minimum energy pathways by following the intrinsic reaction coordinates (IRCs)[25] from the transition states to the reactants and products.

Higher-level single-point calculations were carried out on the structures optimized by the B3LYP-DFT method to obtain more accurate estimates of selected reaction barriers and enthalpies. At the higher-level limit, the (R)CCSD(T)/6-311+G(3df,2p) electronic energy was approximated within a framework of the G2M composite method.[26] Among several versions suitable for systems of different size, the G2M(RCC6) scheme has been chosen for the present molecules containing up to nine carbon atoms

$$E[\text{G2M(RCC6)}] = E[\text{(P)MP4/6-311G(d,p)}] + \Delta E(\text{RCC}) + \Delta E(+3\text{df,2p})$$

$$\Delta E(\text{RCC}) = E[\text{(R)CCSD(T)/6-31G(d,p)}] - E[\text{(P)MP4/6-31G(d,p)}]$$

$$\Delta E(+3\text{df,2p}) = E[\text{(R/U)MP2/6-311+G(3df,2p)}] - E[\text{(R/U)MP2/6-311G(d,p)}]$$

In the above notations, methods with prefixes (P), (R), and (U) differ only for open-shell systems. Specifically, (R)CCSD(T)[27] here denotes a partially spin-adapted open-shell coupled cluster singles and doubles theory augmented with a perturbation correction for triple excitations (MOLPRO keyword RHF-RCCSD(T)); (P)MP4[28] is an approximate spin-projected MP4(SDTQ) energy after annihilation of s + 1 to s + 4 spin states; (R)MP2[29] is a spin-restricted open-shell MP2 (Gaussian keyword ROMP2). The present implementation of the G2M method for open-shell species is slightly different from the original formulas of Mebel et al.[25] in two instances: (1) the basis set extension term $\Delta E(+3\text{df,2p})$ is evaluated by the (R)MP2 method, instead of (U)MP2, and (2) the empirical higher-level corrections (HLCs) defined by the number of α and β valence electrons are omitted. Replacing (U)MP2 with (R)MP2 alleviates the deficiencies of the former method induced by high spin contamination of the UHF reference wave functions for aromatic and delocalized radicals. The second modification is possible because all reactions considered in this study are isogyric, in which case HLCs cancel out in all relative energies. Recently, we have employed the same methodology in the computational studies of the phenyl radical reactions with C_2H_2[8] and C_2H_4[9] and obtained good agreement (typically, within 2 kcal/mol or better) of the calculated energetic parameters with available benchmark values.

Potential Energy Surface. The calculated PES for the reaction of the phenyl radical with propene is schematically depicted in Figure 5. Optimized geometries of the reactants, transition states, and products are given in the Supporting Information. We have explored various reaction pathways on

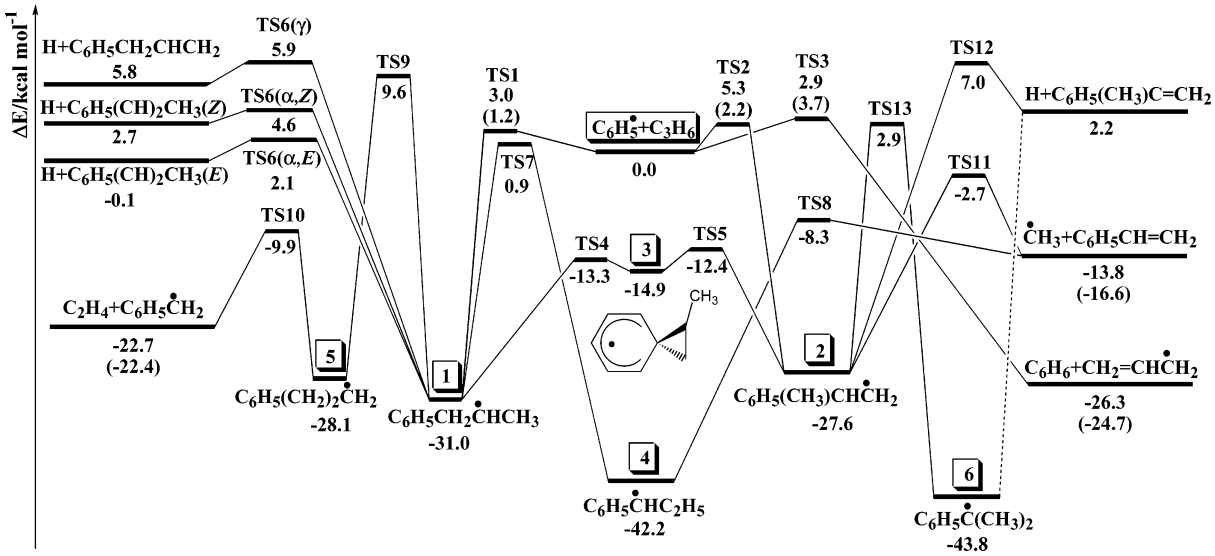

Figure 5. Potential energy diagram for the $C_6H_5 + C_3H_6$ reaction calculated at the B3LYP/6-311++G(d,p) and G2M(RCC6) (in parentheses) levels.

the PES calculated at the B3LYP/6-311++G(d,p) level of theory. The more reliable G2M(RCC6) energy estimates are provided in parentheses in Figure 5 for the most important reaction barriers and enthalpies.

Initially, the reaction of the phenyl radical with propene proceeds via the following three branching channels

$$C_6H_5 + C_3H_6 \rightarrow CH_3CHCH_2C_6H_5\ (\mathbf{1}) \qquad (R1)$$

$$C_6H_5 + C_3H_6 \rightarrow CH_2CH(C_6H_5)CH_3\ (\mathbf{2}) \qquad (R2)$$

$$C_6H_5 + C_3H_6 \rightarrow C_6H_6 + C_3H_5 \qquad (R3)$$

The first two channels describe the C_6H_5 addition to either side of the C=C double bond, producing isomeric CH_3-$CHCH_2C_6H_5$ (**1**) and $CH_2CH(C_6H_5)CH_3$ (**2**) radicals via TS1 and TS2, respectively. The third channel corresponds to the H-abstraction from the methyl group of C_3H_6 by the C_6H_5 radical, producing the allyl radical (CH_2CHCH_2) and benzene via TS3.

According to our best energy estimates obtained for TS1−TS3 by the G2M(RCC6) method, the addition of C_6H_5 at the terminal C-atom in C_3H_6 has the lowest barrier of 1.2 kcal/mol, followed by the C_6H_5 addition at the middle C-atom over a barrier of 2.2 kcal/mol and by the H-abstraction channel (R3) with a barrier of 3.7 kcal/mol. It is instructive to compare these values to the predicted (G2M) barriers for the $C_6H_5 + C_2H_4$ reaction,[9] which were in the range of 2.1−2.3 kcal/mol for the addition channel and ∼9 kcal/mol for the abstraction of the vinylic H-atom. The H-for-CH_3 substitution at the double C=C bond increases the π-electron density at the terminal C-atom, making it a more attractive site for the C_6H_5 radical addition. The much lower barrier for the allylic H-abstraction from C_3H_6 compared with the barrier for the vinylic H-abstraction from C_2H_4 is a consequence of the allylic C−H bond in C_3H_6 ($D_{298}°(CH_2CHCH_2-H) = 87.0 \pm 1.0$ kcal/mol)[30] being much weaker than the vinylic C−H bond in C_2H_4 ($D_{298}°(C_2H_3-H) = 110.7 \pm 0.6$ kcal/mol).[31] The vinylic C−H bonds in C_3H_6 and C_2H_4 have similar bond strengths such that they are much harder to break than the allylic C−H bonds. Therefore, the allyl radical is expected to be the predominant product of reaction R3, while other C_3H_5 isomers, namely, CH_3CHCH and CH_3-CCH_2, may be formed only as minor coproducts. In this study, we have explicitly considered only the most favorable allylic H-abstraction pathway for reaction R3. The relatively small contribution of the vinylic H-abstraction pathways can be estimated using our previous results for the $C_6H_5 + C_2H_4$ reaction.

Since the addition channels (R1−R2) are very exothermic, both radicals **1** and **2** are initially produced in the excited rovibrational states that have sufficient internal energy to undergo several isomerization and decomposition reactions (see Figure 5). These pathways have been mapped out on the [C_9H_{11}] PES calculated at the B3LYP/6-311++G(d,p) level of theory. In their selection, we relied on the results of our recent detailed analysis of the PES and product distribution for the homologous $C_6H_5 + C_2H_4$ reaction,[9] where we have considered a number of additional isomerization possibilities for the initial $C_6H_5CH_2$-CH_2 adducts, such as the [1,3] H-shift, and ortho(C_4)-cyclization reactions, but found most of them kinetically insignificant. The key isomerization and decomposition pathways for radicals **1** and **2** are briefly discussed below.

The most facile transformation for both radicals **1** and **2** is the ipso(C_3)-cyclization, that is, the intramolecular addition of the side chain radical at the ipso-position of the aromatic ring. The ipso(C_3)-cyclizations of both **1** and **2** yield radical **3** via TS4 and TS5, respectively. Radical **3** is a very short-lived intermediate for the [1,2] phenyl migration (the neophyl-like rearrangement) that interconnects radicals **1** and **2**.

Besides ipso(C_3)-cyclyzations, the two other types of reactions that we have considered for **1** and **2** are radical eliminations and [1,2] H-shifts. Radical **1**, $C_6H_5C^{(\alpha)}H_2C^{(\beta)}HC^{(\gamma)}H_3$, with an unpaired electron centered on the β-carbon atom can undergo a C_6H_5 elimination, which is the reverse of the C_6H_5 addition to the terminal C-atom in C_3H_6, and three H-elimination reactions that involve breaking of either C^{α}−H or C^{γ}−H bonds. The H-elimination from the α-position may yield cis(*Z*) and trans(*E*) isomers of 1-phenylpropene via TS6(α,*Z*) and TS6(α,*E*), respectively. The C^{γ}−H bond scission in **1** produces 3-phenylpropene via TS6(γ). As shown in Figure 5, the B3LYP-DFT barriers for these H-elimination pathways are predicted to lie 2.1 (TS6(α,*E*)) to 5.9 kcal/mol (TS6(γ)) above the energy level of the initial reactants ($C_6H_5 + C_3H_6$), making the H-elimination from the α-position in **1** slightly more favorable. This channel, however, may compete with the [1,2] H-shift from C^{α} to C^{β} atoms that converts **1** to the more stable benzyl-type

TABLE 3: External (I_A, I_B, I_C) and Reduced Internal (I_R) Moments of Inertia (in 10^{-40} g cm^2), Symmetry Numbers (n), and Vibrational Frequencies and Hindering Barriers (V_n) for C_6H_5, C_3H_6, TS1, TS2, and TS3

I_A, I_B, I_C	frequencies and hindered rotors
	C_6H_5 ($^2A_1$, $n = 2$)
133.3, 149.4, 282.7	398.6, 424.4, 600.5, 619.1, 665.4, 718.6, 812.2, 891.8, 961.8, 983.7, 986.6, 1014.3, 1048.6, 1071.5, 1174.7, 1175.7, 1301.1, 1324.3, 1460.6, 1467.9, 1570.0, 1626.5, 3155.9, 3162.0, 3174.4, 3176.9, 3187.8
	C_3H_6 ($^1A'$, $n = 3$)
17.9, 90.6, 103.2	(206.6), 426.5, 591.1, 923.4, 942.9, 948.9, 1025.2, 1070.6, 1189.0, 1327.6, 1407.1, 1448.4, 1480.0, 1494.1, 1704.7, 3012.9, 3056.7, 3091.2, 3120.2, 3126.9, 3208.5 $I_R(CH_3) = 3.91$, $V_3 = 1.9$ kcal/mol
	TS1 ($^2A'$, n=6)
230.3, 1071.5, 1215.3,	196i, (17.2), 50.1, 77.6, 120.2, (149.4), 247.4, 397.1, 424.2, 431.4, 579.7, 610.6, 647.1, 682.5, 723.9, 830.0, 877.1, 896.3, 921.3, 942.2, 961.9, 984.1, 986.8, 995.6, 1016.1, 1048.9, 1051.9, 1074.8, 1175.5, 1178.1, 1189.0, 1304.1, 1311.3, 1324.1, 1405.8, 1438.0, 1460.7, 1473.1, 1477.1, 1490.4, 1574.9, 1619.2, 1623.8, 3005.5, 3045.2, 3091.1, 3128.5, 3134.2, 3147.5, 3152.6, 3163.5, 3167.9, 3183.7, 3222.9 $I_R(CH_3) = 5.19$, $V_3 = 1.3$ kcal/mol $I_R(C_6H_5) = 60.6$, $V_2 = 0.45$ kcal/mol
	TS2 ($^2A'$, $n = 6$)
251.0, 899.6, 1058.5	272i, (27.9), 67.6, 98.9, (159.5), 199.4, 253.1, 398.1, 420.2, 438.2, 518.0, 604.2, 611.5, 680.8, 723.6, 832.0, 867.0, 897.3, 899.0, 941.2, 950.4, 963.0, 982.8, 1002.6, 1018.9, 1045.2, 1057.9, 1076.6, 1175.7, 1180.1, 1183.3, 1291.0, 1313.6, 1324.1, 1408.0, 1438.1, 1460.9, 1474.3, 1484.4, 1495.0, 1573.6, 1594.9, 1623.5, 3018.4, 3077.4, 3106.5, 3126.9, 3139.5, 3145.5, 3153.1, 3163.0, 3169.0, 3183.9, 3216.9 $I_R(CH_3) = 5.19$, $V_3 = 1.5$ kcal/mol $I_R(C_6H_5) = 61.3$, $V_2 = 1.2$ kcal/mol
	TS3 ($^2A'$, $n = 2$)
216.9, 1214.6, 1399.8	1078i, (23.6), 39.9, 67.4, (116.6), 178.3, 358.3, 397.5, 422.9, 434.7, 529.7, 612.9, 629.4, 683.4, 726.8, 728.6, 835.5, 904.0, 925.4, 947.3, 965.5, 972.0, 986.0, 1011.9, 1018.5, 1035.4, 1071.1, 1078.7, 1090.6, 1177.5, 1182.9, 1198.2, 1318.1, 1320.8, 1324.5, 1362.8, 1413.1, 1440.3, 1468.9, 1477.2, 1490.8, 1589.1, 1622.3, 1666.2, 3056.6, 3115.7, 3127.1, 3134.3, 3150.7, 3155.1, 3165.4, 3170.5, 3184.1, 3213.6 $I_R(C_6H_5) = 52.7$, $V_2 = 0.75$ kcal/mol $I_R(C_2H_3) = 25.9$, $V_1 = 4.0$ kcal/mol

radical **4** via TS7. According to the B3LYP-DFT estimates, TS7 is ~1 kcal/mol lower in energy than TS6(α,*E*). In turn, radical **4** is most likely to decompose to styrene and methyl radical via TS8. Another possible [1,2] H-shift in **1** can involve a H-transfer from C^{γ} to C^{β} atoms. This rearrangement converts **1** to radical **5** but has a considerably higher barrier (TS9) than that controlling the H-shift from C^{α} atom via TS7. Radical **5** can break down to C_2H_4 and benzyl radical over the low-lying TS10. However, this channel cannot be easily accessed from radical **1** because of the relatively high barrier (TS9) separating it from radical **5**.

Similar to **1**, the radical center in **2** ($C_6H_5(CH_3)C^{(\alpha)}HC^{(\beta)}H_2$) is on the β-carbon atom of the side chain, which allows for similar types of radical eliminations and H-shifts to take place in both isomers. Since the β-position is terminal in **2**, the radical eliminations there can only occur from the C^{α} atom by breaking of either $C^{\alpha}-CH_3$, or $C^{\alpha}-H$, or $C^{\alpha}-C_6H_5$ bonds (the last reaction is the reverse of the radical **2** formation pathway from $C_6H_5 + C_3H_6$). The $C^{\alpha}-CH_3$ bond is the weakest among the above three bonds which is reflected in the lower barrier for the CH_3 elimination from **2** (TS11) compared with the barriers for the H and C_6H_5 eliminations (TS12 and TS2), as shown in Figure 5. The [1,2] H-shift from the C^{α} to C^{β} atom in **2** has a relatively high barrier (TS13) and is not expected to be competitive with the CH_3-elimination pathway.

We should comment that the isomerization and decomposition pathways for radicals **1** and **2** presented in Figure 5 and discussed above have been studied at the B3LYP/6-311++G-(d,p) level of theory, affordable for the present system. This level of theory, however, may not provide chemically accurate predictions of the energetic parameters. For example, the deviations of the B3LYP values of the initial reaction barriers (TS1−TS3) from the more reliable G2M(RCC6) estimates range from −1.2 kcal/mol for TS3, to +1.8 kcal/mol for TS1, to +3.1 kcal/mol for TS2. Nevertheless, we believe some qualitative conclusions can be drawn about the mechanism of the C_6H_5 addition to C_3H_6. Radicals **1** and **2** initially formed by the C_6H_5 addition to the C=C bond in C_3H_6 can interconvert by the neophyl-like rearrangement pathway. Among various other isomerization and decomposition channels originating from either **1** or **2**, the CH_3 elimination from radical **2** is expected to be the most favorable pathway, especially at high *T*, because it involves a looser transition state than those for the [1,2] H-shifts and H-eliminations from either **1** or **2**.

Theoretical Kinetic Calculations. To quantitatively evaluate the product branching for the $C_6H_5 + C_3H_6$ reaction, detailed Rice−Ramsperger−Kassel−Marcus (RRKM)/master equation modeling needs to be performed for the addition channels to properly account for the effects of pressure and collisional energy transfer in the chemically activated intermediates. Also, additional higher-level calculations are needed to provide more reliable energetic parameters. No experimental data on product branching is currently available for the $C_6H_5 + C_3H_6$ reaction that could be used for benchmarking the global [C_9H_{11}] PES. Therefore, we have not pursued the detailed kinetic modeling of the $C_6H_5 + C_3H_6$ reaction in this work. Instead, we have

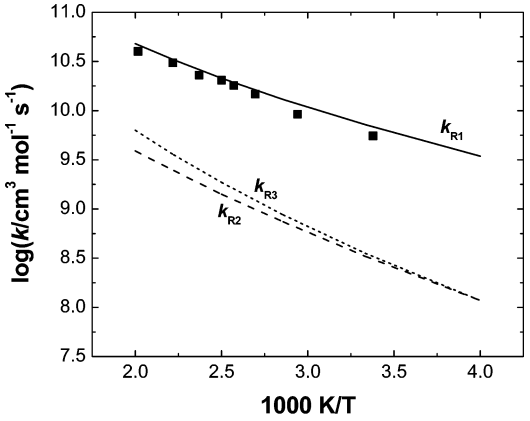

Figure 6. Arrhenius plot of the $k(C_6H_5 + C_3H_6)$ rate constant: experimental (■) and calculated values (lines).

limited the extent of our theoretical kinetic calculations to the evaluation of the total rate constant and initial product branching between channels (R1−R3) at the high-pressure limit (HPL).

The rate constant calculations were carried out by canonical transition state theory[32] with hindered rotor treatment[33] and unsymmetric Eckart tunneling corrections,[34] as implemented in the ChemRate program.[35] The B3LYP/6-311++G(d,p) optimized molecular parameters listed in Table 3 were used in the partition function calculations. The standard rigid rotor harmonic oscillator formalism was used to calculate the external rotational and vibrational partition functions, excluding those for large amplitude (low frequency) torsional modes, which were treated as hindered 1-D internal rotations. The hindering barriers were estimated from the corresponding torsional frequencies,[36] assuming a sinusoidal form of the torsional potential. Reduced moments of inertia for internal rotations were calculated by the method of Pitzer and Gwinn.[32]

Our experimental results indicate that under the conditions of our CRDS measurements ($T < 500$ K, $P > 40$ Torr) the total rate constant for all modes of the $C_6H_5 + C_3H_6$ reaction (R1−R3) is near the HPL. Hence, it can be evaluated by the conventional TST as a sum of the branching rate constants, $k(C_6H_5 + C_3H_6) = k_{R1} + k_{R2} + k_{R3}$. The branching rate constants calculated from the G2M energetic and B3LYP/6-311++G(d,p) molecular parameters (Table 3) can be given by the following expressions (in units of $cm^3\ mol^{-1}\ s^{-1}$) at $T = 250-2500$ K

$$k_{R1} = 1.70 \times 10^4 T^{2.47} \exp[-370/T]$$

$$k_{R2} = 1.60 \times 10^3 T^{2.64} \exp[-847/T]$$

$$k_{R3} = 1.36 T^{3.82} \exp[-723/T]$$

The calculated $k(C_6H_5 + C_3H_6)$ is shown together with the experimental data from this work in Figure 6. Without empirical adjustments of any sort, the calculated total rate constant exhibits an excellent correlation with experimental results (the theoretical predictions are up to 30% higher than the experimental values). The total rate constant is dominated by k_{R1}, although the H-abstraction mode (R3) becomes increasingly important at higher T. The contribution of k_{R3} to $k(C_6H_5 + C_3H_6)$ increases from 5% at 300 K to 13% at 500 K.

Conclusions

The reaction of C_6H_5 with propylene has been studied by CRDS at temperatures 296−496 K under an Ar pressure of 40 Torr. The total rate constant has been measured for the first time and interpreted as a sum of addition and abstraction modes (R1−R3) with a dominant contribution of the C_6H_5 addition to the terminal carbon atom, which is in agreement with the conclusions of the earlier low-T ESR study.[14]

Acknowledgment. The authors are grateful for the support of this work from the Department of Energy, Office of Basic Energy Sciences, Division of Chemical Sciences through Contract DE-FGO2-97ER14784. Also, we are thankful to the Cherry L. Emerson Center of Emory University for the use of its resources, which is in part supported by National Science Foundation Grant CHE-0079627 and an IBM Shared University Research Award. M.C.L. also acknowledges the support form Taiwan National Science Council for a distinguished visiting professorship at the Center for Interdisciplinary Molecular Science, National Chiao Tung University, Hsinchu, Taiwan.

Supporting Information Available: Optimized geometries (cartesian coordinates in angstroms) of the reactants, transition states, and products of the $C_6H_5 + C_3H_6$ reaction are listed in Table S1. This material is available free of charge via the Internet at http://pubs.acs.org.

References and Notes

(1) Frenklach, M. *Phys. Chem. Chem. Phys.* **2002**, *4*, 2028−2037.
(2) Richter, H.; Howard, J. B. *Prog. Energy Combust. Sci.* **2000**, *26*, 565−608.
(3) Lindstedt, P.; Maurice, L.; Meyer, M. *Faraday Discuss.* **2001**, *119*, 409−432.
(4) Miller, J. A.; Pilling, M. J.; Troe, J. *Proc. Combust. Inst.* **2005**, *30*, 43−88.
(5) Frenklach, M.; Feigelson, E. D. *Astrophys. J.* **1989**, *341*, 372.
(6) Kaiser, R. I. *Chem. Rev.* **2002**, *102*, 1309.
(7) Yu, T.; Lin, M. C. *J. Phys. Chem.* **1994**, *98*, 2105. Yu, T.; Lin, M. C. *J. Am. Chem. Soc.* **1994**, *116*, 9571.
(8) Tokmakov, I. V.; Lin, M. C. *J. Am. Chem. Soc.* **2003**, *125*, 11397−11408.
(9) Tokmakov, I. V.; Lin, M. C. *J. Phys. Chem. A* **2004**, *108*, 9697−9714.
(10) Tokmakov, I. V.; Park, J.; Lin, M. C. *ChemPhysChem* **2005**, *6* (10), 2075−2085.
(11) Kaiser, R. I.; Asvany, O.; Lee, Y. T.; Bettinger, H. F.; Schleyer, P. v. R.; Schaefer, H. F., III. *J. Chem. Phys.* **2000**, *112*, 4994−5001.
(12) Vereecken, L.; Peeters, J.; Bettinger, H. F.; Kaiser, R. I.; Schleyer, P. v. R.; Schaefer, H. F., III. *J. Am. Chem. Soc.* **2002**, *124*, 2781−2789.
(13) Vereecken, L.; Bittinger, H. F.; Peeters, J. *Phys. Chem. Chem. Phys.* **2002**, *4*, 2019−2027.
(14) Hefter, H. J.; Hecht, T. A.; Hammond, G. S. *J. Am. Chem. Soc.* **1972**, *94*, 2793−2797.
(15) Porter, G.; Ward, B. *Proc. R. Soc. London, Ser. A* **1965**, *287*, 457.
(16) Tonokura, K.; Norikane, Y.; Koshi, M.; Nakano, Y.; Nakamichi, S.; Goto, M.; Hashimoto, S.; Kawasaki, M.; Sulbaek Andersen, M. P.; Hurley, M. D.; Wallington, T. J. *J. Phys. Chem. A* **2002**, *106*, 5908.
(17) Tokmakov, I. V.; Park, J.; Gheyas, S.; Lin, M. C. *J. Phys. Chem. A* **1999**, *103*, 3636−3645.
(18) NIST Standard Reference Database, 17-2Q98.
(19) Lutz, A. E.; Kee, R. J.; Miller, J. A. *SENKIN: A FORTRAN Program for Predicting Homogeneous Gas-Phase Chemical Kinetics with Sensitivity Analysis*; Report No. SAND87-8248; Sandia National Laboratories: Albuquerque, NM, 1988.
(20) Frisch, M. J.; Trucks, G. W.; Schlegel, H. B.; Scuseria, G. E.; Robb, M. A.; Cheeseman, J. R.; Montgomery, J. A., Jr.; Vreven, T.; Kudin, K. N.; Burant, J. C.; Millam, J. M.; Iyengar, S. S.; Tomasi, J.; Barone, V.; Mennucci, B.; Cossi, M.; Scalmani, G.; Rega, N.; Petersson, G. A.; Nakatsuji, H.; Hada, M.; Ehara, M.; Toyota, K.; Fukuda, R.; Hasegawa, J.; Ishida, M.; Nakajima, T.; Honda, Y.; Kitao, O.; Nakai, H.; Klene, M.; Li, X.; Knox, J. E.; Hratchian, H. P.; Cross, J. B.; Adamo, C.; Jaramillo, J.; Gomperts, R.; Stratmann, R. E.; Yazyev, O.; Austin, A. J.; Cammi, R.; Pomelli, C.; Ochterski, J. W.; Ayala, P. Y.; Morokuma, K.; Voth, G. A.; Salvador, P.; Dannenberg, J. J.; Zakrzewski, V. G.; Dapprich, S.; Daniels, A. D.; Strain, M. C.; Farkas, O.; Malick, D. K.; Rabuck, A. D.; Raghavachari, K.; Foresman, J. B.; Ortiz, J. V.; Cui, Q.; Baboul, A. G.; Clifford, S.; Cioslowski, J.; Stefanov, B. B.; Liu, G.; Liashenko, A.; Piskorz, P.; Komaromi, I.; Martin, R. L.; Fox, D. J.; Keith, T.; Al-Laham, M. A.; Peng, C. Y.; Nanayakkara, A.; Challacombe, M.; Gill, P. M. W.; Johnson,

B.; Chen, W.; Wong, M. W.; Gonzalez, C.; Pople, J. A. *Gaussian 03*, Revision B.01; Gaussian, Inc.: Pittsburgh, PA, 2003.

(21) Amos, R. D.; Bernhardsson, A.; Berning, A.; Celani, P.; Cooper, D. L.; Deegan, M. J. O.; Dobbyn, A. J.; Eckert, F.; Hampel, C.; Hetzer, G.; Knowles, P. J.; Korona, T.; Lindh, R.; Lloyd, A. W.; McNicholas, S. J.; Manby, F. R.; Meyer, W.; Mura, M. E.; Nicklass, A.; Palmieri, P.; Pitzer, R.; Rauhut, G.; Schütz, M.; Schumann, U.; Stoll, H.; Stone, A. J.; Tarroni, R.; Thorsteinsson, T.; Werner, H.-J. *MOLPRO*, version 2002.6; University of Birmingham: Birmingham, UK, 2003.

(22) Becke, A. D. *J. Chem. Phys*. **1993**, *98*, 5648. Becke, A. D. *Phys. Rev. A* **1988**, *38*, 3098. Lee, C.; Yang, W.; Parr, R. G. *Phys. Rev. B* **1988**, *37*, 785. Stephens, P. J.; Devlin, F. J.; Chabalowski, C. F.; Frisch, M. J. *J. Phys. Chem*. **1994**, *98*, 11623.

(23) Peng, C.; Ayala, P. Y.; Schlegel, H. B.; Frisch, M. J. *J. Comput. Chem.* **1996**, *17*, 49.

(24) (a) Csaszar, P.; Pulay, P. *J. Mol. Struct. (THEOCHEM)* **1984**, *114*, 31. (b) Farkas, O.; Schlegel, H. B. *J. Chem. Phys.* **1999**, *111*, 10806.

(25) (a) Gonzalez, C.; Schlegel, H. B. *J. Chem. Phys*. **1989**, *90*, 2154−2161. (b) Gonzalez, C.; Schlegel, H. B. *J. Phys. Chem*. **1990**, *94*, 5523−5527.

(26) Mebel, A. M.; Morokuma, K.; Lin, M. C. *J. Chem. Phys*. **1995**, *103*, 7414.

(27) (a) Knowles, P. J.; Hampel, C.; Werner, H. J. *J. Chem. Phys*. **1993**, *99*, 5219−5227 and refs therein. (b) Knowles, P. J.; Hampel, C.; Werner, H. J. *J. Chem. Phys*. **2000**, *112*, 3106−7. (c) Watts, J. D.; Gauss, J.; Bartlett, R. J. *J. Chem. Phys*. **1993**, *98*, 8718.

(28) Chen, W.; Schlegel, H. B. *J. Chem. Phys*. **1994**, *101*, 5957−5968.

(29) Knowles, P. J.; Andrews, J. S.; Amos, R. D.; Handy, N. C.; Pople, J. A. *Chem. Phys. Lett*. **1991**, *186*, 130.

(30) Seetula, J. A. *Phys. Chem. Chem. Phys*. **1999**, *1* (20), 4727−4731.

(31) Ervin, K. M.; DeTuri, V. F. *J. Phys. Chem. A* **2002**, *106*, 9947.

(32) Laidler, K. J. *Chemical Kinetics*, 3rd ed.; Harper and Row: New York, 1987.

(33) Pitzer, K. S. *J. Chem. Phys*. **1946**, *14*, 239. Pitzer, K. S.; Gwinn, W. D. *J. Chem. Phys*. **1942**, *10*, 428.

(34) Eckart, C. *Phys. Rev*. **1930**, *35*, 1303.

(35) Mokrushin, V.; Bedanov, V.; Tsang, W.; Zachariah, M.; Knyazev, V. *ChemRate*, version 1.19; NIST: Gaithersburg, MD, 2002.

(36) Forst, W. *Unimolecular Reactions: A Concise Introduction*; Cambridge University Press: New York, 2003; p 72.